Geomechanics and Engineering, *Vol. 19, No. 3 (2019) 201-215*
DOI: https://doi.org/10.12989/gae.2019.19.3.201

Elastic solutions for shallow tunnels excavated under non-axisymmetric displacement boundary conditions on a vertical surface

Ling Wang[1,2], Jin-Feng Zou[1], Tao Yang*[1] and Feng Wang[1]

[1]*School of Civil Engineering, Central South University, No.22, Shaoshan South Road, Central South University Railway Campus, Changsha, Hunan Province, People's Republic of China*
[2]*Department of Environmental Design, Hunan University of Technology and business, No. 8 569, Yuelu Road, Hunan University of Technology and Business, Changsha, Hunan Province, People's Republic of China*

(Received January 16, 2019, Revised September 27, 2019, Accepted October 11, 2019)

Abstract. A new approach of analyzing the displacements and stress of the surrounding rock for shallow tunnels excavated under non-axisymmetric displacement boundary conditions on a vertical surface is investigated in this study. In the proposed approach, by using a virtual image technique, the shear stress of the vertical ground surface is revised to be zero, and elastic solutions of the surrounding rock are obtained before stress revision. To revise the vertical normal stress and shear stress of horizontal ground surface generated by the combined action of the actual and image sinks, the harmonic functions and corresponding stress function solutions were adopted. Based on the Boussinesq's solutions and integral method, the horizontal normal stress of the vertical ground surface is revised to be zero. Based on the linear superposition principle, the final solution of the displacements and stress were proposed by superimposing the solutions obtained by the virtual image technique and the stress revision on the horizontal and vertical ground surfaces. Furthermore, the ground settlements and lateral displacements of the horizontal and vertical ground surfaces are derived by the proposed approach. The proposed approach was well verified by comparing with the numerical method. The discussion based on the proposed approach in the manuscript shows that smaller horizontal ground settlements will be induced by lower tunnel buried depths and smaller limb distances. The proposed approach for the displacement and stress of the surrounding rocks can provide some practical information about the surrounding rock stability analysis of shallow tunnels excavated under non-axisymmetric displacement boundary conditions on a vertical surface.

Keywords: shallow tunnel; non-axisymmetric displacement boundary; virtual image technique; linear superposition principle; ground settlement

1. Introduction

The accurate prediction of stresses and displacements around a circular opening is important for ensuring the stability of tunnel excavations (Wang *et al.* 2019). The study of the face stability of circular tunnels has been investigated by several scholars in the previous work using different methods: (a) analytical methods on the basis of the limit analysis method (e.g., Chen *et al.* 2019a, b, Mollon *et al.* 2011, 2013, Oreste and Dias 2012, Zhang *et al.* 2015, Zou *et al.* 2019a, b, Pan and Dias 2017, 2018, Daraei and Zare 2018, Huang *et al.* 2018, Han *et al.* 2016, Li and Yang 2019, Zhang *et al.* 2018), (b) numerical analysis (e.g., Fahimifar *et al.* 2015, Zou *et al.* 2016, Xiao *et al.* 2017a, b, Zou *et al.* 2019c, d), and (c) experimental investigations (Broere and Van 2000, Zou *et al.* 2018). Some scholars (Brown *et al.* 1983, Alonso *et al.* 2003) have illustrated that compared to the cavity expansion theory (Li *et al.* 2019a, b), it is more reliable to study the developments of the stresses and strains of rock masses surrounding tunnels by using the cavity contraction theory. Farmer and Glossop (1979) obtained observations in planes normal to the tunnel center axis during tunnel constructions, removing the stabilizing air pressure 25 days after construction in the infinite space. Yu and Houlsby (1995) adopted the non-associated Mohr-Coulomb yield criterion to derive the solution of the cylindrical and spherical cavity contraction in an infinite space. Brown *et al.* (1983) presented methods of response curve calculations for a circular tunnel excavated in an infinite space subjected to a hydrostatic in situ stress field. Lee and Pietruszczak (2008) studied the excavation of a circular tunnel in strain-softening materials by a finite difference method. Wang *et al.* (2010) presented an approach for analyzing circular tunnel excavations in an infinite space.

As mentioned above, many researchers have been devoted to tunnel stability analysis and prediction of stresses and displacements for a tunnel excavated in an infinite space. In addition, the problem of a semi-infinite space has also been investigated by several scholars. For example, Peck (1969) proposed a prediction approach for the transverse settlement curve of a tunnel. Wood (1975) established the loading on a circular tunnel in the elliptical mode of deformation near the ground surface. Sagataseta (1987) proposed closed-form solutions for obtaining the strain field in an initially isotropic and homogeneous incompressible soil due to near-surface ground loss. Considering ground loss and the oval deformation of a

*Corresponding author, Ph.D. Student
E-mail: yangtao@csu.edu.cn

ISSN: 2005-307X (Print), 2092-6219 (Online)

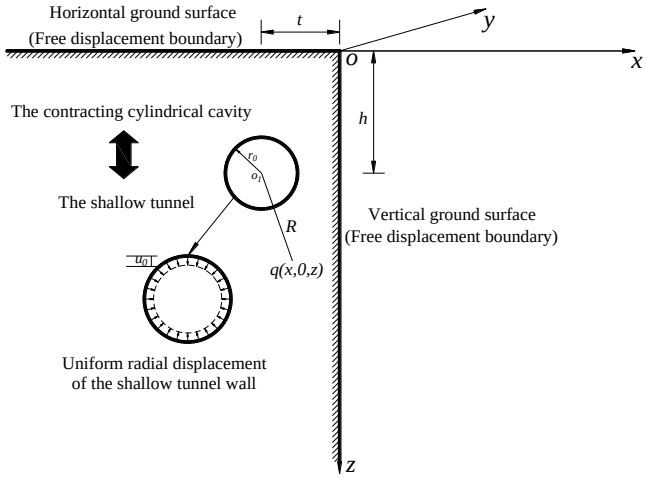

Fig. 1 Mechanical model of a shallow tunnel excavated under non-axisymmetric displacement boundary conditions on a vertical surface

tunnel, Verejijt and Booker (1996) provided an approximate solution for isotropic and compressible soil masses in an elastic half space on the basis of Sagataseta's solution. Verruijt (1997) presented an analytical solution for an elastic half-plane of a circular tunnel by using complex variables and a conformal mapping onto a circular ring. Verruijt (1998) developed an analytical solution for solving the problems of an elastic half plane of a circular cavity by adopting a complex function method. Loganathan and Poulos (1998) incorporated an equivalent ground loss parameter with respect to the gap parameters to obtain analytical solutions for predicting the ground movements around a tunnel in clay soils. Yu and Rowe (1999) derived analytical and semianalytical solutions of unloading cylindrical and spherical cavities for in situ state of stress under both drained and undrained conditions. Boet (2001) presented complete analytical solutions for a shallow tunnel in the saturated ground of a semi-infinite space. Park (2004) presented elastic solutions for the prediction of the tunneling-induced ground deformations for shallow and deep tunnels in soft ground. However, none of the above studies considered the boundary effects of a vertical surface on the displacement and stresses around the surrounding rock of shallow tunnels.

In contrast with the above research findings in the symmetric infinite and semi-infinite spaces, only a limited number of literature reports have been presented for the cavity expansion problem under non-axisymmetric displacement boundary conditions. For example, Li *et al.* (2013) presented an analytical solution of cavity expansion near sloping ground by the introduction of a virtual image technique, the harmonic function and the Boussinesq solution. Zou and Zuo (2017) proposed similar solutions for the synchronous grouting of shielded tunnels by considering the boundary effects of the non-axisymmetric displacement boundary on vertical surfaces. However, no literature reports and solutions have been presented for the surrounding rock stability analysis problem of shallow tunnels that are excavated under non-axisymmetric displacement boundary conditions on a vertical surface. Bias tunneling is an indispensable and common part of tunnel engineering practice. Currently, most of the theoretical research on tunnel stability is based on the symmetric infinite space or semi-infinite space, which is widely used in ordinary tunnel stability analysis. However, in regard to bias tunnel, all of the presented approaches lose their applicability. Thus, this paper proposes a new approach for the stability analysis of shallow tunnels excavated under non-axisymmetric displacement boundary conditions on a vertical surface. In this study, displacements and stresses of the surrounding rock masses, the ground settlement and lateral horizontal displacements of the horizontal and vertical surfaces can be obtained by adopting the virtual image technique, the harmonic function and the corresponding stress function solutions, Boussinesq's solutions and the linear superposition principle. In addition, the proposed approach is useful in various situations that include the stability assessments of circular openings such as excavated bias tunnels, the verification of numerical codes, etc. It can be applied to the prediction of the ground settlement and lateral displacement of the horizontal and vertical ground surfaces for bias tunnel engineering. In brief, the proposed approach can provide some practical suggestions for site selections of bias tunnels and deformation monitoring of the surrounding rock of shallow tunnels that are excavated under non-axisymmetric displacement boundary conditions.

2. Problem statement

As Fig. 1 shows, a shallow tunnel, o_1, with an excavation radius, r_o, limb distance, t, and the tunnel buried depth, h, is excavated under the non-axisymmetric displacement boundary conditions on a vertical surface. Because the excavation process of the shallow tunnel, o_1, is finished under non-axisymmetric displacement boundary conditions on a vertical surface (see Fig. 1), a radial contracting displacement, u_0, is produced around the shallow tunnel wall. Taking the intersection point of the horizontal ground surface and the inclined surface as the origin point o, a rectangular xyz space coordinate system is

established. Moreover, the non-axisymmetric displacement boundary conditions on a vertical surface mean that there are no normal stresses and no shear stresses in the horizontal ground surface (i.e., at z=0) and the vertical ground surface (i.e., at x=0).

3. Assumptions

To reduce the difficulties of the theoretical analysis and solve this problem more conveniently, the following assumptions were made for computing the displacements and stresses around shallow tunnels, the displacements of the horizontal ground surface and the displacements of the vertical ground surface.

(1) The surrounding rock is assumed to be homogeneous, incompressible and isotropic, which satisfies the small deformation hypothesis and Hooke's law.

(2) The deformation of the surrounding rock of the shallow tunnel is assumed to be a displacement-displacement problem.

(3) The gravity effect on the surrounding rock is neglected.

(4) The excavation process of shallow tunnels can be assumed to be a cylindrical cavity contraction problem under the plane-strain condition.

(5) The geometric shape of shallow tunnels is assumed to be circular, and the location of the shallow tunnel center is assumed to not change.

(6) The radial contracting displacement, u_0, is assumed to be the maximum value of the vault settlement, which is induced by the tunnel excavation process.

(7) The positive directions of the displacement and the stress are in agreement with the positive directions of the x, y and z axes in the space rectangular coordinate system.

4. Methodology

4.1 Research scheme

A new approach for determining the displacements and stress is being proposed in terms of the virtual image technique, the harmonic function, the stress function solution and Boussinesq's solution for the cylindrical cavity contraction problem under non-axisymmetric displacement boundary conditions on a vertical surface. The specific research thoughts are clearly shown as follows.

(1) Based on the elastic mechanics theory and the virtual image technique, the first part of the displacements and stress of the surrounding rock are obtained before stress revision. The virtual image technique includes a negative virtual image and a positive virtual image. The latter is adopted in the solving process, so the virtual image technique presented in this paper refers to the positive virtual image technique.

(2) To obtain the second part of the displacements and stress of the surrounding rock, which is generated by the vertical normal stress revision on the horizontal ground surface, the harmonic function and corresponding stress function solutions in spatial rectangular coordinate system are adopted.

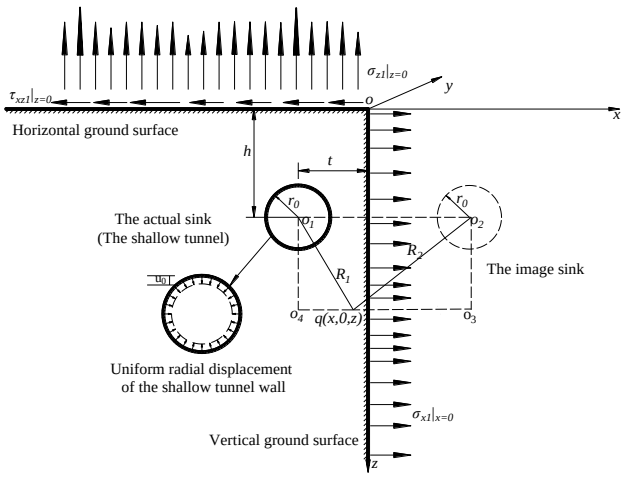

Fig. 2 Mechanical model of the cylindrical cavity contraction problem before stress revision under non-axisymmetric displacement boundary conditions on a vertical surface

(3) In the same way, the harmonic function and corresponding stress function solutions in spatial rectangular coordinate system are adopted to calculate the third part of the displacements and stress of the surrounding rock, which are generated by the shear stress revision on the horizontal ground surface.

(4) The fourth part of the displacements and stress of the surrounding rock, which are induced by the horizontal normal stress revision of the vertical ground surface, are obtained through the coordinate conversion formula, Boussinesq's solution and integrating method.

(5) The final displacements and stress of the surrounding rock for shallow tunnels under the nonsymmetric displacement boundary condition on vertical surface are proposed by the linear superposition principle from step (1) to step (4).

(6) By substituting z=0 into the horizontal and vertical displacement formula of point $q(x,0,z)$, the ground settlements and lateral displacements of horizontal ground surface can be derived.

(7) The ground settlements and lateral displacements of vertical ground surface can be derived by substituting x=0 into the horizontal and vertical displacement formula of point $q(x,0,z)$.

4.2 Elastic solutions of the surrounding rocks

4.2.1 Elastic solutions of the surrounding rock before stress correction

Fig. 2 is a mechanical model of the cylindrical cavity contraction problem under non-axisymmetric displacement boundary conditions on a vertical surface. Under the combined influence of the actual sink, o_1, and the image sink, o_2, the nonuniform vertical normal stress, $\sigma_{z1}|_{z=0}$, and the shear stress, $\tau_{xz1}|_{z=0}$, is produced on the horizontal ground surface, and only the nonuniform vertical normal stress, $\sigma_{x1}|_{x=0}$, is produced on the vertical ground surface.

Based on the geometric relationships shown in Fig. 2, R_1 and R_2 can be given by

$$R_1=\sqrt{(x+t)^2+(z-h)^2} \tag{1}$$

$$R_2=\sqrt{(x-t)^2+(z-h)^2} \tag{2}$$

where R_1 is the distance between the center of the actual sink, o_1, and the calculation point $q(x,0,z)$, and R_2 is the distance between the center of the image sink, o_2, and the calculation point $q(x,0,z)$.

When the boundary influences of the horizontal and vertical ground surface are not considered, the first part of the displacements of the calculation point $q(x,0,z)$, which is based on the well-known solutions originating from the elasticity theory (Timoshenko and Goodier 1970). These can be expressed as follows

$$U_{x1}=\text{-}u_0r_0\left(\frac{x+t}{R_1^{\,2}}+\frac{x-t}{R_2^{\,2}}\right) \tag{3}$$

$$U_{z1}=\text{-}u_0r_0\left(\frac{z-h}{R_1^{\,2}}+\frac{z-h}{R_2^{\,2}}\right) \tag{4}$$

where U_{x1}, U_{z1} are the first parts of the horizontal and vertical displacements of the calculation point $q(x,0,z)$, respectively.

Based on the geometric equation and physical equation of the plane strain problem in the elastic mechanics (Timoshenko and Goodier 1970), the stress solutions of the calculation point $q(x,0,z)$ can be derived without any stress revision as follows

$$\sigma_{x1}=-2Gu_0r_0\left[\frac{1}{R_1^2}-\frac{2(x+t)^2}{R_1^4}+\frac{1}{R_2^2}-\frac{2(x-t)^2}{R_2^4}\right] \tag{5}$$

$$\sigma_{z1}=-2Gu_0r_0\left[\frac{1}{R_1^2}-\frac{2(z-h)^2}{R_1^4}+\frac{1}{R_2^2}-\frac{2(z-h)^2}{R_2^4}\right] \tag{6}$$

$$\sigma_{y1}=0 \tag{7}$$

$$\tau_{xz1}=\tau_{zx1}=4Gu_0r_0\left[\frac{(x+t)(z-h)}{R_1^4}+\frac{(x-t)(z-h)}{R_2^4}\right] \tag{8}$$

where σ_{x1}, σ_{z1} and τ_{xz1} are the first part of the horizontal and vertical, axial normal stresses and the shear stress of calculation point $q(x,0,z)$, respectively. E is elastic modulus of the soil mass, v is Poisson's ratio of soil mass, and G is the shear modulus of the soil mass (i.e., $G=\frac{E}{2(1+v)}$).

From Eqs. (6) and (8), the vertical normal stress and shear stress on the horizontal ground surface, which is induced by the combined action of the actual sink and the image sink, can be expressed as follows

$$\sigma_{z1}\big|_{z=0}=-2Gu_0r_0\left[\frac{(x+t)^2-h^2}{\left((x+t)^2+h^2\right)^2}+\frac{(x-t)^2-h^2}{\left((x-t)^2+h^2\right)^2}\right]\neq 0 \tag{9}$$

$$\tau_{xz1}\big|_{z=0}=-4Gu_0r_0\left\{\frac{(x+t)h}{\left[(x+t)^2+h^2\right]^2}+\frac{(x-t)h}{\left[(x-t)^2+h^2\right]^2}\right\}\neq 0 \tag{10}$$

Similarly, under the combined effect of the actual sink and image sink, the nonzero horizontal normal stress on the vertical ground surface can be obtained by substituting x=0 into Eq. (5) as follows

$$\sigma_{x1}\big|_{x=0}=-4Gu_0r_0\left[\frac{(z-h)^2-t^2}{\left(t^2+(z-h)^2\right)^2}\right]\neq 0 \tag{11}$$

4.2.2 Vertical normal stress correction on horizontal ground surface

To eliminate the vertical normal stress, $\sigma_{z1}\big|_{z=0}$, on the horizontal ground surface, the stress function solutions (Kassir and Sih 1975) that are helpful solving the elasticity problem that satisfies the above boundary condition (i.e., $\sigma_{z2}\big|_{z=0}=-\sigma_{z1}\big|_{z=0}$ and $\tau_{xz2}\big|_{z=0}=0$) are expressed as follows

$$U_{x2}=(1-2v)\frac{\partial f}{\partial x}+z\frac{\partial^2 f}{\partial x\partial z} \tag{12}$$

$$U_{z2}=-2(1-v)\frac{\partial f}{\partial z}+z\frac{\partial^2 f}{\partial z^2} \tag{13}$$

$$\sigma_{x2}=2G\left[\frac{\partial^2 f}{\partial x^2}+z\frac{\partial^3 f}{\partial x^2\partial z}\right] \tag{14}$$

$$\sigma_{y2}=4Gv\frac{\partial^2 f}{\partial x^2} \tag{15}$$

$$\sigma_{z2}=2G\left[-\frac{\partial^2 f}{\partial z^2}+z\frac{\partial^3 f}{\partial z^3}\right] \tag{16}$$

$$\tau_{zx2}=\tau_{xz2}=2Gz\frac{\partial^3 f}{\partial x\partial z^2} \tag{17}$$

Based on the harmonic function condition of $\nabla^2 f=0$, the harmonic function f can be defined as follows

$$f=A(\ln R_3+\ln R_4) \tag{18}$$

where A is an undetermined constant that can be solved by the free displacement boundary condition that there is null vertical normal stress on the ground surface.

In addition, R_3 and R_4 can be expressed as follows, respectively

$$R_3=\sqrt{(x+t)^2+(z+h)^2} \tag{19}$$

$$R_4=\sqrt{(x-t)^2+(z+h)^2} \tag{20}$$

where R_3 is the distance between the calculation point and the center location of the actual sink with respect to the horizontal ground surface, and R_4 is the distance between the calculation point and the center location of the image sink with respect to the horizontal ground surface.

By substituting Eq. (18) and z=0 into the stress function solution (Kassir and Sih, 1975), the vertical normal stress on the horizontal ground surface, induced by the vertical normal stress correction on the horizontal ground surface, can be obtained as follows

$$\sigma_{z2}\big|_{z=0}=-2GA\left[\frac{(x+t)^2-h^2}{\left((x+t)^2+h^2\right)^2}+\frac{(x-t)^2-h^2}{((x-t)^2+h^2)^2}\right] \tag{21}$$

As a consequence, the vertical normal stress on the horizontal ground surface can be eliminated by the harmonic function f with a suitable value of the constant A. Combining Eq. (9), Eq. (21) and $\sigma_{z2}\big|_{z=0}=-\sigma_{z1}\big|_{z=0}$, it leads to

$$-2GA\left[\frac{(x+t)^2-h^2}{\left((x+t)^2+h^2\right)^2}+\frac{(x-t)^2-h^2}{((x-t)^2+h^2)^2}\right]=2Gu_0r_0\left[\frac{(x+t)^2-h^2}{\left((x+t)^2+h^2\right)^2}+\frac{(x-t)^2-h^2}{\left((x-t)^2+h^2\right)^2}\right] \tag{22}$$

Solving Eq. (16) results in

$$A=-u_0r_0 \tag{23}$$

By substituting Eq. (23) into the stress function solution (Kassir and Sih 1975), the second part of the displacements and stress of the calculation point $q(x,0,z)$ induced by the vertical normal stress correction on the horizontal ground surface, are obtained as follows

$$U_{x2}=-u_0r_0\left[\begin{array}{l}\dfrac{(1-2\nu)(x+t)}{R_3^2}-\dfrac{2z(x+t)(z+h)}{R_3^4}\\ +\dfrac{(1-2\nu)(x-t)}{R_4^2}-\dfrac{2z(x-t)(z+h)}{R_4^4}\end{array}\right] \tag{24}$$

$$U_{z2}=-u_0r_0\left[\begin{array}{l}-\dfrac{2(1-\nu)(z+h)}{R_3^2}+\dfrac{z}{R_3^2}-\dfrac{2z(z+h)^2}{R_3^4}\\ -\dfrac{2(1-\nu)(z+h)}{R_4^2}+\dfrac{z}{R_4^2}-\dfrac{2z(z+h)^2}{R_4^4}\end{array}\right] \tag{25}$$

$$\sigma_{x2}=-2Gu_0r_0\left[\begin{array}{l}\dfrac{1-4\nu}{R_3^2}-\dfrac{2z(z+h)}{R_3^4}+\dfrac{8(x+t)^2z(z+h)}{R_3^6}\\ +\dfrac{1-4\nu}{R_4^2}-\dfrac{2z(z+h)}{R_4^4}+\dfrac{8(x-t)^2z(z+h)}{R_4^6}\end{array}\right] \tag{26}$$

$$\sigma_{y2}=-2Gu_0r_0\left[\begin{array}{l}\dfrac{x+t}{xR_3^2}+\dfrac{2\nu}{R_3^2}-\dfrac{4\nu(x+t)^2}{R_3^4}-\dfrac{2(x+t)z(z+h)}{R_3^4}\\ +\dfrac{x-t}{xR_4^2}+\dfrac{2\nu}{R_4^2}-\dfrac{4\nu(x-t)^2}{R_4^4}-\dfrac{2(x-t)z(z+h)}{R_4^4}\end{array}\right] \tag{27}$$

$$\sigma_{z2}=-2Gu_0r_0\left[\begin{array}{l}-\dfrac{1}{R_3^2}+\dfrac{2(z+h)^2-6z(z+h)}{R_3^4}+\dfrac{8z(z+h)^3}{R_3^6}\\ -\dfrac{1}{R_4^2}+\dfrac{2(z+h)^2-6z(z+h)}{R_4^4}+\dfrac{8z(z+h)^3}{R_4^6}\end{array}\right] \tag{28}$$

$$\tau_{xz2}=-2Gu_0r_0\left[\begin{array}{l}-\dfrac{2(x+t)z}{R_3^4}+\dfrac{8(x+t)(z+h)^2z}{R_3^6}\\ -\dfrac{2(x-t)z}{R_4^4}+\dfrac{8(x-t)(z+h)^2z}{R_4^6}\end{array}\right] \tag{29}$$

4.2.3 Shear stress correction on the horizontal ground surface

To eliminate the shear stress on the horizontal ground surface, the series of functions (Kassir and Sih 1975) that can help solve the elasticity problem under the following boundary conditions (i.e., $\tau_{xz3}\big|_{z=0}=-\tau_{xz1}\big|_{z=0}$ and $\sigma_{z3}\big|_{z=0}=0$) are given as follows

$$U_{x3}=2(1-\nu)\frac{\partial g}{\partial x}+z\frac{\partial^2 g}{\partial x\partial z} \tag{30}$$

$$U_{z3}=-(1-2\nu)\frac{\partial g}{\partial z}+z\frac{\partial^2 g}{\partial z^2} \tag{31}$$

$$\sigma_{x3}=2G\left(2\frac{\partial^2 g}{\partial x^2}+z\frac{\partial^3 g}{\partial x^2\partial z}\right) \tag{32}$$

$$\sigma_{y3}=4G\nu\frac{\partial^2 g}{\partial x^2} \tag{33}$$

$$\sigma_{z3}=2Gz\frac{\partial^3 g}{\partial z^3} \tag{34}$$

$$\tau_{xz3}=\tau_{zx3}=2G\left(\frac{\partial^2 g}{\partial x\partial z}+z\frac{\partial^3 g}{\partial x\partial z^2}\right) \tag{35}$$

In the same way, to satisfy the harmonic function condition of $\nabla^2 g=0$, the harmonic function g can also be determined by

$$g=B\left(\ln R_3+\ln R_4\right) \tag{36}$$

where B is an undetermined constant, which could be solved by the condition of a null shear stress on the horizontal ground surface.

Likewise, the shear stress on the horizontal ground surface $\tau_{xz3}\big|_{z=0}$, applied to eliminate the shear stress $\tau_{xz1}\big|_{z=0}$, can be calculated by substituting Eq. (36) and z=0 into the stress function solution (Kassir and Sih 1975) as follows

$$\tau_{xz3}\big|_{z=0}=-4GB\left\{\frac{(x+t)h}{\left[\left(x+t\right)^2+h^2\right]^2}+\frac{(x-t)h}{\left[\left(x-t\right)^2+h^2\right]^2}\right\} \tag{37}$$

Consequently, the shear stress, which is caused by the combined influence of the actual sink and image sink, can be balanced by obtaining a suitable value for the constant B. Combining Eq. (10), Eq. (37) and $\tau_{xz3}\big|_{z=0}=-\tau_{xz1}\big|_{z=0}$,

results in

$$-4GB\left\{\frac{(x+t)h}{\left[(x+t)^2+h^2\right]^2}+\frac{(x-t)h}{\left[(x-t)^2+h^2\right]^2}\right\} = 4Gu_0r_0\left\{\frac{(x+t)h}{\left[(x+t)^2+h^2\right]^2}+\frac{(x-t)h}{\left[(x-t)^2+h^2\right]^2}\right\} \tag{38}$$

The undetermined constant B can be obtained by solving Eq. (38) as follows

$$B=-u_0r_0 \tag{39}$$

By substituting Eq.(39) into the stress function solution (Kassir and Sih 1975), the third part of the displacements and stress of the calculation point $q(x,0,z)$ generated from the shear stress revision of the horizontal ground surface, are obtained as follows

$$U_{x3}=-u_0r_0\left[\frac{2(1-\nu)(x+t)}{R_3^2}-\frac{2z(x+t)(z+h)}{R_3^4}+\frac{2(1-\nu)(x-t)}{R_4^2}-\frac{2z(x-t)(z+h)}{R_4^4}\right] \tag{40}$$

$$U_{z3}=-u_0r_0\left[-\frac{(1-2\nu)(z+h)}{R_3^2}+\frac{z}{R_3^2}-\frac{2z(z+h)^2}{R_3^4}-\frac{(1-2\nu)(z+h)}{R_4^2}+\frac{z}{R_4^2}-\frac{2z(z+h)^2}{R_4^4}\right] \tag{41}$$

$$\sigma_{x3}=-2Gu_0r_0\left[\frac{2}{R_3^2}-\frac{4(x+t)^2}{R_3^4}-\frac{2\nu(x+t)}{xR_3^2}-\frac{2z(z+h)}{R_3^4}+\frac{8(x+t)^2z(z+h)}{R_3^6}+\frac{2}{R_4^2}-\frac{4(x-t)^2}{R_4^4}-\frac{2\nu(x-t)}{xR_4^2}-\frac{2z(z+h)}{R_4^4}+\frac{8(x-t)^2z(z+h)}{R_4^6}\right] \tag{42}$$

$$\sigma_{y3}=-2Gu_0r_0\left[\frac{x+t}{xR_3^2}+\frac{2\nu}{R_3^2}-\frac{4\nu(x+t)^2}{R_3^4}-\frac{2(x+t)z(z+h)}{R_3^4}+\frac{x-t}{xR_4^2}+\frac{2\nu}{R_4^2}-\frac{4\nu(x-t)^2}{R_4^4}-\frac{2(x-t)z(z+h)}{R_4^4}\right] \tag{43}$$

$$\sigma_{z3}=-2Gu_0r_0\left[\frac{8z(z+h)^3}{R_3^6}-\frac{6z(z+h)^2}{R_3^2}+\frac{8z(z+h)^3}{R_4^6}-\frac{6z(z+h)^2}{R_4^2}\right] \tag{44}$$

$$\tau_{xz3}=-2Gu_0r_0\left[-\frac{2(x+t)(z+h)}{R_3^4}-\frac{2(x+t)z}{R_3^4}+\frac{8(x+t)(z+h)^2z}{R_3^6}-\frac{2(x-t)(z+h)}{R_4^4}-\frac{2(x-t)z}{R_4^4}+\frac{8(x-t)(z+h)^2z}{R_4^6}\right] \tag{45}$$

4.2.4 Horizontal normal stress revision on the vertical ground surface

As shown in Fig. 3, it can be known that an equivalent distribution of the horizontal force, $\sigma_{x0}(0,0,\rho)$, are applied to balance the horizontal normal stress, $\sigma_{x1}|_{x=0}$, induced by

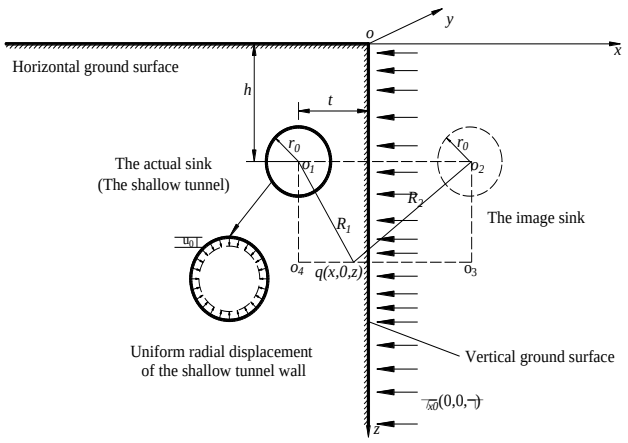

Fig. 3 Horizontal normal stress correction on the vertical ground surface

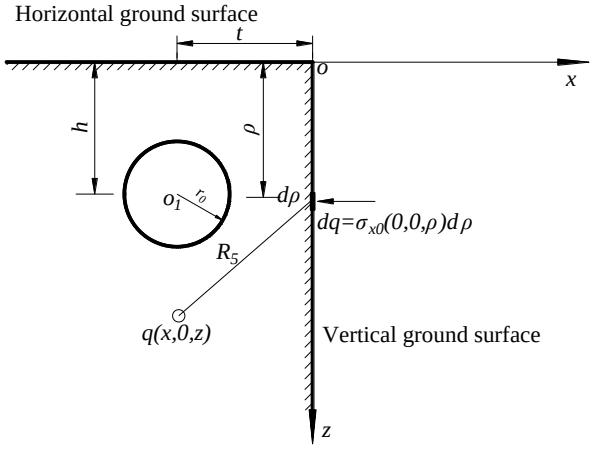

Fig. 4 Horizontal normal stress calculation of the vertical ground surface

the combined action of the actual sink and the image sink. The following solutions are adopted to correct the horizontal normal stress $\sigma_{x1}|_{x=0}$ of the vertical ground surface.

To eliminate the horizontal normal stress on the vertical ground surface, an equivalent horizontal distribution stress with the opposite direction of the horizontal normal stress is applied to the vertical ground surface. In addition, the expression of the applied horizontal distribution stress can be obtained by the combined derivation of Eq. (11) and $\sigma_{x0}(0,0,\rho)=-\sigma_{x1}|_{\substack{x=0\\z=\rho}}$, as follows

$$\sigma_{x0}(0,0,\rho)=\frac{4Gu_0r_0\left[(\rho-h)^2-t^2\right]}{\left(t^2+(\rho-h)^2\right)^2} \tag{46}$$

where ρ is the vertical coordinate of the nonuniform distributed stress, the range of ρ values is $(0,10h)$, and $\sigma_{x0}(0,0,\rho)$ is the applied horizontal distribution stress at point $q(0,0,\rho)$ of the vertical ground surface.

The stress and displacement at point $q(x,0,z)$, affected by nonuniform horizontal distributed force, will be obtained by the means of the integral method and the Boussinesq's solution (see Eqs. (47)-(52)).

$$U_x=\frac{(1+\mu)P}{2\pi ER}\left[\frac{xz}{R^2}-\frac{(1-2\mu)x}{R+z}\right] \tag{47}$$

$$U_z=\frac{(1+\mu)P}{2\pi ER}\left[2(1-\mu)+\frac{z^2}{R^2}\right] \tag{48}$$

$$\sigma_x=\frac{P}{2\pi R^2}\left[\frac{(1-2\mu)R}{R+z}-\frac{3x^2z}{R^3}\right] \tag{49}$$

$$\sigma_y=\frac{(1-2\mu)P}{2\pi R^2}\left(\frac{z}{R}-\frac{R}{R+z}\right) \tag{50}$$

$$\sigma_z=-\frac{3Pz^3}{2\pi R^5} \tag{51}$$

$$\tau_{xz}=\tau_{zx}=-\frac{3Pxz^2}{2\pi R^5} \tag{52}$$

As shown in Fig. 4, the area micro unit is determined in the range of the horizontal distribution force and is equal to be the line micro unit (i.e., $dA=d\rho$). Therefore, the horizontal concentrated force of the area micro unit dq, which is applied to the vertical ground surface, can be expressed as $dq=\sigma_{x0}(0,0,\rho)d\rho$. In addition, R_5 is the distance between the calculation point $q(x,0,z)$ and the loading position of the horizontal concentrated force (i.e., $R_5=\sqrt{x^2+(z-\rho)^2}$).

Based on the Boussinesq's solution (Boussinesq 1885) and the coordinated transformation formulas of displacements and stress, the fourth part of the displacements and stress at point $q(x,0,z)$, which are generated by the all horizontal concentrated forces dq from 0 to $10h$, can be solved by the integral method as follows

$$U_{x4}=-\int_0^{10h}\frac{(1+\nu)}{2\pi ER_5}\left[2(1-\nu)+\frac{x^2}{R_5{}^2}\right]\sigma_{x0}(0,0,\rho)d\rho \tag{53}$$

$$U_{z4}=\int_0^{10h}\frac{(1+\nu)}{2\pi ER_5}\left[-\frac{zx}{R_5{}^2}-\frac{(1-2\nu)z}{R_5-x}\right]\sigma_{x0}(0,0,\rho)d\rho \tag{54}$$

$$\sigma_{x4}=\int_0^{10h}\frac{3x^3}{2\pi R_5{}^5}\sigma_{x0}(0,0,\rho)d\rho \tag{55}$$

$$\sigma_{y4}=\int_0^{10h}\frac{(1-2\nu)}{2\pi R_5{}^2}\left(-\frac{x}{R_5}-\frac{R_5}{R_5-x}\right)\sigma_{x0}(0,0,\rho)d\rho \tag{56}$$

$$\sigma_{z4}=\int_0^{10h}\frac{1}{2\pi R_5{}^2}\left[\frac{(1-2\nu)R_5}{R_5-x}+\frac{3xz^2}{R_5{}^3}\right]\sigma_{x0}(0,0,\rho)d\rho \tag{57}$$

$$\tau_{xz4}=\int_0^{10h}\frac{3zx^2}{2\pi R_5{}^5}\sigma_{x0}(0,0,\rho)d\rho \tag{58}$$

where U_{x4}, and U_{z4} are the fourth parts of the horizontal and vertical displacements of calculation point $q(x,0,z)$, respectively; and σ_{x4}, σ_{y4}, σ_{z4} and τ_{xz4} are the fourth parts of the horizontal, axial, vertical normal stress and shear stress at the calculation point $q(x,0,z)$, respectively.

4.2.5 Elastic solutions of the surrounding rock after stress correction

Based on the linear superposition principle (Timoshenko and Goodier 1970), the final displacements and stress of the calculation point $q(x,0,z)$ of the surrounding rock can be derived by the superposition of Eqs. (3) to (8), (24) to (28), (40) to (45) and (53) to (58) as follows, respectively

$$U_x=U_{x1}+U_{x2}+U_{x3}+U_{x4} \tag{59}$$

$$U_z=U_{z1}+U_{z2}+U_{z3}+U_{z4} \tag{60}$$

$$\sigma_x=\sigma_{x1}+\sigma_{x2}+\sigma_{x3}+\sigma_{x4} \tag{61}$$

$$\sigma_y=\sigma_{y1}+\sigma_{y2}+\sigma_{y3}+\sigma_{y4} \tag{62}$$

$$\sigma_z=\sigma_{z1}+\sigma_{z2}+\sigma_{z3}+\sigma_{z4} \tag{63}$$

$$\tau_{xz}=\tau_{xz1}+\tau_{xz2}+\tau_{xz3}+\tau_{xz4} \tag{64}$$

4.3 Displacements of the horizontal ground surface

According to the Eqs. (59) and (60), the full solutions of the ground settlement and the lateral displacement of the horizontal ground surface can be expressed as follows

$$U_x(x,0,0)=U_{x1}(x,0,0)+U_{x2}(x,0,0)+U_{x3}(x,0,0)+U_{x4}(x,0,0) \tag{65}$$

$$U_z(x,0,0)=U_{z1}(x,0,0)+U_{z2}(x,0,0)+U_{z3}(x,0,0)+U_{z4}(x,0,0) \tag{66}$$

By substituting z=0 into the Eqs. (3) and (4), the first part of the ground settlement and lateral displacement at point $q(x,0,0)$, induced by the combined action of the actual and image sinks, can be obtained as follows

$$U_{x1}(x,0,0)=-u_0r_0\left[\frac{x+t}{(x+t)^2+h^2}+\frac{x-t}{(x-t)^2+h^2}\right] \tag{67}$$

$$U_{z1}(x,0,0)=u_0r_0\left[\frac{h}{(x+t)^2+h^2}+\frac{h}{(x-t)^2+h^2}\right] \tag{68}$$

And the second part of the ground settlement and lateral displacement at point $q(x,0,0)$, which is induced by the vertical normal stress revision on the horizontal ground surface, can be derived by substituting z=0 into the Eqs. (24)-(25)

$$U_{x2}(x,0,0)=-u_0r_0\left[\frac{(1-2\nu)(x+t)}{(x+t)^2+h^2}+\frac{(1-2\nu)(x-t)}{(x-t)^2+h^2}\right] \tag{69}$$

$$U_{z2}(x,0,0)=2u_0r_0\left[\frac{(1-\nu)h}{(x+t)^2+h^2}+\frac{(1-\nu)h}{(x-t)^2+h^2}\right] \tag{70}$$

In the shear stress revision process of the horizontal

ground surface, the third part of the ground settlement and lateral displacement at point $q(x,0,0)$ can be determined by substituting z=0 into Eqs. (40) and (41) as follows

$$U_{x3}(x,0,0)=-2u_0r_0\left[\frac{(1-v)(x+t)}{(x+t)^2+h^2}+\frac{(1-v)(x-t)}{(x-t)^2+h^2}\right] \tag{71}$$

$$U_{z3}(x,0,0)=u_0r_0\left[\frac{(1-2v)h}{(x+t)^2+h^2}+\frac{(1-2v)h}{(x-t)^2+h^2}\right] \tag{72}$$

Under the horizontal normal stress revision of the vertical ground surface, the fourth part of the ground settlement and lateral displacement at point $q(x,0,0)$ can be obtained by substituting z=0 into Eqs. (53) and (54) as follows

$$U_{x4}(x,0,0)=-\int_0^{10h}\frac{(1+v)}{2\pi E\sqrt{x^2+\rho^2}}\left[2(1-v)+\frac{x^2}{x^2+\rho^2}\right]\sigma_{x0}(0,0,\rho)d\rho \tag{73}$$

$$U_{z4}(x,0,0)=0 \tag{74}$$

By substituting Eqs. (67), (69), (71) and (73) into the Eq. (65), the final solution of lateral displacement at point $q(x,0,0)$ can be expressed as follows

$$\begin{aligned}U_x(x,0,0)=&-4(1-v)u_0r_0\left[\frac{(x+t)}{(x+t)^2+h^2}+\frac{(x-t)}{(x-t)^2+h^2}\right]\\&-\int_0^{10h}\frac{(1+v)}{2\pi E\sqrt{x^2+\rho^2}}\left[2(1-v)+\frac{x^2}{x^2+\rho^2}\right]\sigma_{x0}(0,0,\rho)d\rho\end{aligned} \tag{75}$$

Likewise, the final solution of ground settlement at point $q(x,0,0)$ can be expressed by substituting Eqs. (68), (71), (72) and (74) into the Eq. (66) as follows

$$U_z(x,0,0)=4(1-v)u_0r_0\left[\frac{h}{(x+t)^2+h^2}+\frac{h}{(x-t)^2+h^2}\right] \tag{76}$$

Eqs. (75) and (76) can be well applied in the prediction of the lateral displacement and ground settlement on the horizontal ground surface induced by shallow tunnel excavations under non-axisymmetric displacement boundary on vertical surface.

4.4 Displacements on the vertical ground surface

Initially, the first part of the ground settlement and lateral displacement at point $q(0,0,z)$, which is induced by the combined influence of the actual and image sinks, can be expressed by substituting x=0 into Eqs. (3) and (4), as follows

$$U_{x1}(0,0,z)=0 \tag{77}$$

$$U_{z1}(0,0,z)=-2u_0r_0\frac{(z-h)}{t^2+(z-h)^2} \tag{78}$$

In the vertical normal stress revision process on the horizontal ground surface, the second part of the ground settlement and lateral displacement at point $q(0,0,z)$, can be obtained by substituting x=0 into Eqs. (24) and (25) as follows

$$U_{x2}(0,0,z)=0 \tag{79}$$

$$U_{z2}(0,0,z)=2u_0r_0\left[\frac{2(1-v)(z+h)}{t^2+(z+h)^2}-\frac{z}{t^2+(z+h)^2}+\frac{2z(z+h)^2}{\left(t^2+(z+h)^2\right)^2}\right] \tag{80}$$

By substituting x=0 into the Eqs. (40) and (41), the third part of the ground settlement and lateral displacement of point $q(0,0,z)$, which is induced by the shear stress revision of the horizontal ground surface, can be derived as shown in Eqs. (81) and (82).

$$U_{x3}(0,0,z)=0 \tag{81}$$

$$U_{z3}(0,0,z)=2u_0r_0\left[\frac{(1-2v)(z+h)}{t^2+(z+h)^2}-\frac{z}{t^2+(z+h)^2}+\frac{2z(z+h)^2}{\left(t^2+(z+h)^2\right)^2}\right] \tag{82}$$

Likewise, the fourth part of the ground settlement and lateral displacement at point $q(0,0,z)$, produced by the horizontal normal stress revision process of the vertical ground surface, can be calculated by substituting x=0 into the Eqs. (53) and (54) as follows

$$U_{x4}(0,0,z)=-\int_0^{10h}\frac{(1-v^2)}{\pi E|z-\rho|}\sigma_{x0}(0,0,\rho)d\rho \tag{83}$$

$$U_{z4}(0,0,z)=-\int_0^{10h}\frac{(1+v)(1-2v)z}{2\pi E(z-\rho)^2}\sigma_{x0}(0,0,\rho)d\rho \tag{84}$$

Based on Eqs. (59) and (60), the final solutions of the ground settlement and lateral displacement on the vertical ground surface can be obtained as follows

$$U_x(0,0,z)=U_{x1}(0,0,z)+U_{x2}(0,0,z)+U_{x3}(0,0,z)+U_{x4}(0,0,z) \tag{85}$$

$$U_z(0,0,z)=U_{z1}(0,0,z)+U_{z2}(0,0,z)+U_{z3}(0,0,z)+U_{z4}(0,0,z) \tag{86}$$

By substituting Eqs. (77), (79), (81) and (83) into Eq. (85), the final horizontal displacement at point q(x,0,0) can be derived as follows

$$U_x(0,0,z)=-\int_0^{10h}\frac{(1-v^2)}{\pi E|z-\rho|}\sigma_{x0}(0,0,\rho)d\rho \tag{87}$$

Likewise, the final vertical displacement at point q(x,0,0) can be obtained by substituting Eqs. (78), (80), (82) and (84) into the Eq. (86) as follows

$$\begin{aligned}U_z(0,0,z)=&-2u_0r_0\frac{(z-h)}{t^2+(z-h)^2}+2u_0r_0\left[\frac{(3-4v)(z+h)}{t^2+(z+h)^2}-\frac{2z}{t^2+(z+h)^2}+\frac{4z(z+h)^2}{\left(t^2+(z+h)^2\right)^2}\right]\\&-\int_0^{10h}\frac{(1+v)(1-2v)z}{2\pi E(z-\rho)^2}\sigma_{x0}(0,0,\rho)d\rho\end{aligned} \tag{88}$$

The Eqs. (87) and (88) can be well applied in the prediction of the ground settlement and lateral displacement of the vertical ground surface when shallow tunnels are excavated under non-axisymmetric displacement boundary conditions on a vertical surface.

5. Validation

Local test results are used to validate the effectiveness of the proposed approach. The results calculated by the

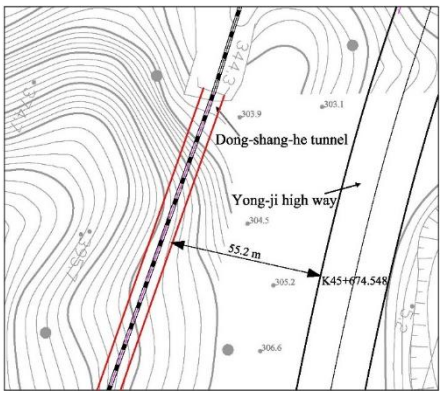

Fig. 5 Topographic map of the Dong-shang-he tunnel

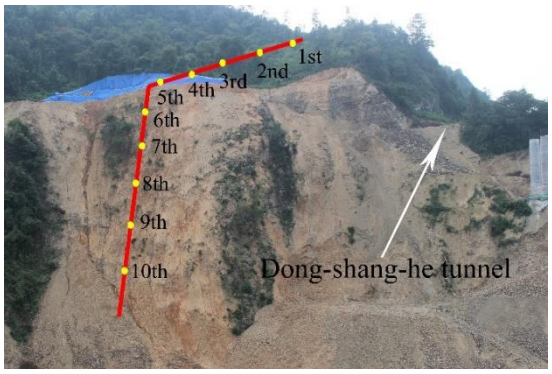

Fig. 7 The field measuring points of the Dong-shang-he tunnel

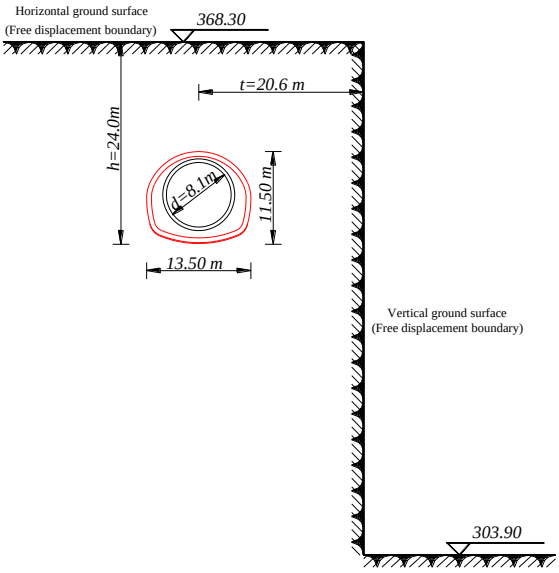

Fig. 6 Cross sectional (K25+360) diagram of the Dong-shang-he tunnel

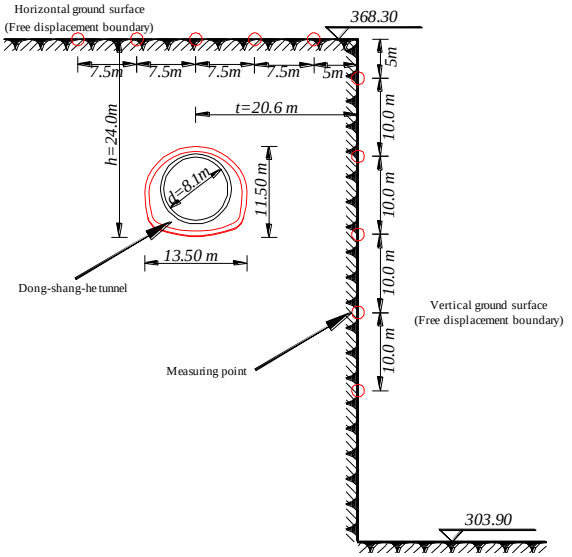

Fig. 8 The simplified measuring point arrangement diagram of the Dong-shang-he tunnel

proposed approach are used to predict the horizontal ground settlement and the horizontal displacement on vertical surface, and compared with the numerical result of the finite element method as well as the field measurement data in Dong-shang-he tunnel.

5.1 Validation with the local test results

5.1.1 Engineering conditions

Since the field measured data of the horizontal displacement of the vertical surface were taken from the Dong-shang-he tunnel, some basic engineering conditions of the Dong-shang-he tunnel are introduced here as follows. The Dong-shang-he tunnel is located in the northern mountainous area of Guzhang County that is in the Xiangxi autonomous prefecture of the Hunan Province of China. The total length of the Dong-shang-he tunnel is 205.0 m; the maximum buried depth of the Dong-shang-he tunnel is 24.0 m; and the rock surrounding the tunnel is grade Ⅴ. A topographic map and cross-sectional diagram of the Dong-shang-he tunnel are shown in Fig. 5 and Fig. 6, respectively.

5.1.2 Arranging conditions of measuring point

To obtain the field measured data of the horizontal ground settlement induced by the tunnel excavation, five measuring points (the 1st to 5th) were arranged on the horizontal ground surface of cross section (K25+360) of the Dong-shang-he tunnel. Likewise, to obtain the field measured data of the horizontal displacement of the vertical surface induced by the tunnel excavation, five measuring points (the 6th to the 10th) were arranged on the vertical surface of cross section (K25+360) of the Dong-shang-he tunnel. The specific measuring point arranging condition of the measuring points and the geometric information of the Dong-shang-he tunnel are shown in Fig. 7 and Fig. 8, respectively.

5.1.3 Calculation parameters

As shown in Fig. 8 of Section 5.1, some of the geometric parameters are as follows: r0=6.25 m, h=24 m and t=20.6 m.

Based on the measured crown settlement field data of cross section (K25+360) of the Dong-shang-he tunnel, the value of the uniform radial contracting displacement is u0=0.036 m.

Because the surrounding rock of the Dong-shang-he is grade Ⅴ, the value of the elastic modulus and Poisson's

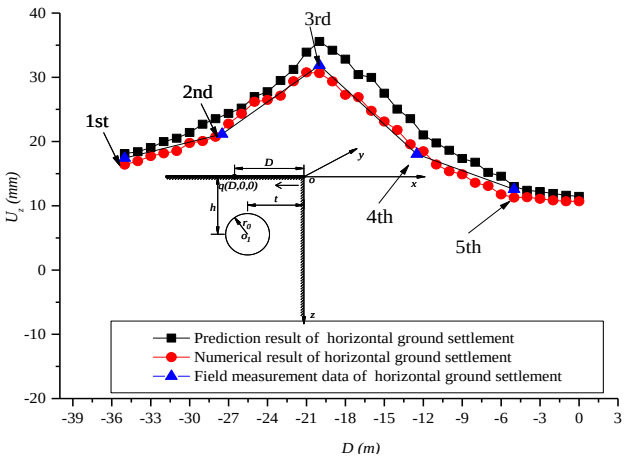

Fig. 9 Comparisons of the horizontal ground settlement

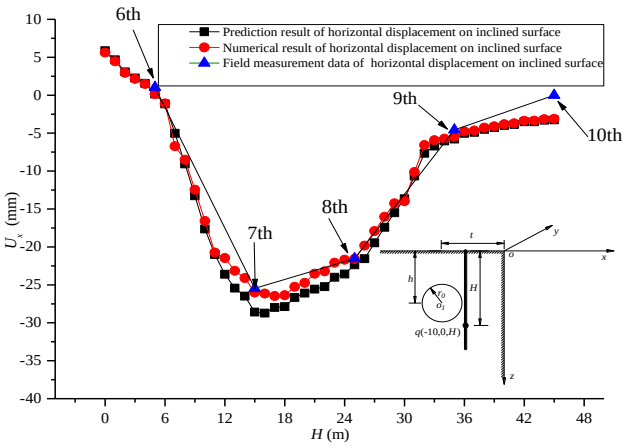

Fig. 10 Comparison of the horizontal displacement results of vertical surface

ratio of the Dong-shang-he tunnel are as follows: E=1.5 GPa, and v=0.45, respectively.

5.1.4 Horizontal ground settlement

The results calculated by the proposed approach, the numerical method and the field test data of the horizontal ground settlements are shown in Fig. 9.

As seen Fig. 9, with the increase of "D" from -35 m to 0 m, the variation trends of the three methods (i.e., the proposed approach, the numerical method and the field measuring method) are consistent. The horizontal ground settlement first increases gradually and then decreases. On the one hand, the maximum difference of the horizontal ground settlement does not exceed 9.72% between the prediction result and the field measurement data. On the other hand, the maximum difference of the horizontal ground settlement does not exceed 9.85% between the theoretical solution and the numerical result. For example, the values of the theoretical solution of the horizontal ground settlement are larger than those of the field measured data by 6.55%, 9.60%, 9.72%, 9.14% and 5.50% from the 1st measuring point to the 5th measuring point, respectively. In addition, the values of the ground settlement predicted by the proposed method are larger than those of the numerical result by 7.51%, 9.09%, 9.85%, 8.67% and 7.88% from the 1st measuring point to the 5th measuring point, respectively. The two comparisons show that the prediction approach of the horizontal ground settlement can be used to ensure more safety for shallow tunnels excavation. Therefore, the rationality and validity of the proposed approach for predicting displacements on horizontal ground surface are well verified by the filed measuring data.

5.1.5 Horizontal displacement of the inclined surface

The prediction results calculated by the proposed approach, the numerical result of the numerical method as well as the field measured data of Dong-shang-he tunnel for horizontal displacement of the vertical surface are shown in Fig. 10.

It can be inferred from Fig. 10 that with the increase of "H" from 5 m to 45 m. the variation trends of the three methods (i.e., the proposed approach, the numerical method and the field measuring method) are consistent. In addition, the differences of the horizontal displacements of the vertical surface are small between the prediction results and the measured field data. For example, the horizontal displacement values of the inclined surface by the proposed approach are larger than those of the field measured data by 7.68%, 9.63%, 8.66%, 9.33% and 9.32% from the 6th to 9th measuring points, respectively. Since the abnormality of the 10th measuring point value is zero, we do not compare it in this article. Moreover, the differences of the horizontal displacement values of the vertical surface do not exceed 9.23% between the prediction results and the numerical results. For instance, the horizontal displacement values of the vertical surface of the proposed approach are larger than those of the numerical result by 6.16%, 9.23%, 7.89%, 6.76% and 5.12% from the 6th to the 10th measuring points, respectively. The two comparisons show that the prediction approach of the horizontal displacements of the vertical surface can be used to ensure more safety for shallow tunnels excavation. Therefore, the rationality and validity of the proposed approach for predicting displacements on vertical surface are well verified by the measured field data.

5.2 Validation with the numerical method

To validate the rationality and suitability of the proposed approach, a finite-element model of a shallow tunnel that is excavated under the non-axisymmetric displacement boundary conditions on a vertical surface was established using the ABAQUS finite element software with a uniform radial contraction displacement, u_0, as shown in Fig. 11. To investigate the effect of gravity, two simulations of this finite element model, with and without considering gravity, respectively, were carried out to calculate the stress and displacements. The left and bottom boundaries are fixed where the horizontal and vertical displacements are zero. Moreover, the lengths of the left, right, bottom, and top boundaries are all set equal to 150 m. The plane-strain condition is adopted in the grid unit division of the FEM model. In addition, the calculation parameters, which originate from the Heathrow tunnel (Loganathan and Poulos 1998), are shown as follows: h=19 m, t=15 m, r_0=4.25 m, u_0=0.058 m, E=35 MPa, and v=0.5.

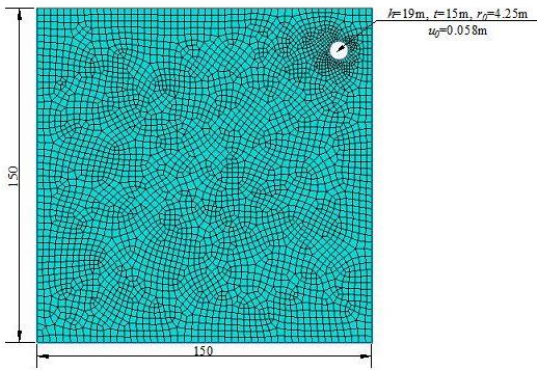

Fig. 11 FEM model of a shallow tunnel excavation under non-axisymmetric displacement boundary conditions

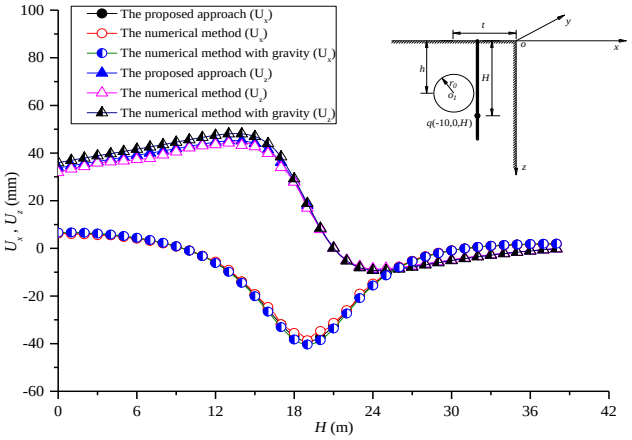

Fig. 12 Displacements calculated by two methods on the right of the shallow tunnel

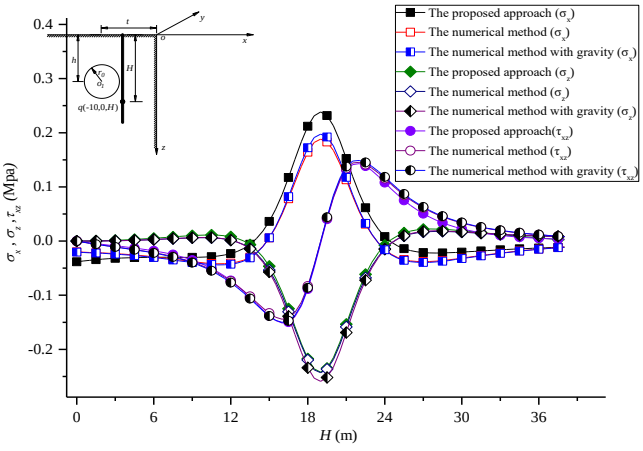

Fig. 13 Stress obtained by two methods on the right side of the shallow tunnel

5.2.1 Displacements and stress on the right side of the shallow tunnel

Fig. 12 and Fig. 13 show that displacements and stress of the surrounding rock solved by the proposed approach and the numerical method at calculation point on the right side of the shallow tunnel, respectively, where H is the vertical coordinate on the right side of the shallow tunnel.

As shown in Fig. 12, the variation trends of the horizontal and vertical displacements at point q (-10, 0, H) calculated by the proposed approach agree well with those calculated by the numerical method. In addition, the differences of the horizontal and vertical displacements between the proposed approach and the numerical method are small. For example, the maximum differences of the horizontal and vertical displacements calculated by the two methods are 7.86% and 7.76%, respectively. Therefore, the rationality and validity of the proposed approach for calculating displacements on the right side of shallow tunnels are well verified by the numerical simulation results. As shown in Fig. 12, gravity has a slight effect on the displacements, and its influence on the vertical displacement is larger than its influence on the horizontal displacement. The average differences of the horizontal and vertical displacements calculated by the numerical method (considering gravity and ignoring gravity) are 3.61% and 6.52%, respectively.

As Fig. 13 shows, the variation trend of the vertical normal stresses (σ_z) and the shear stresses (τ_{xz}) calculated by the proposed approach agree well with those calculated by the numerical method. In addition, the differences are negligible. For example, the maximum difference of the vertical normal stress between the two methods is 0.45%, while this figure for the shear stress is 1.71%. In addition, the variation trend of the horizontal normal stresses (σx) calculated by the proposed approach is consistent with the numerical simulation results. When the depth is less than 6 m, the differences of the horizontal normal stresses are negligible between the proposed approach and the numerical results. However, when the depth exceeds 6 m (H>6 m), the corresponding differences are relatively large, reaching 8.51%. In brief, the proposed approach is more conservative as H<6 m and more suited to deal with tunnel engineering problems when lacking engineering experience. Since the variation trend of the stresses calculated by the proposed approach are consistent with the numerical results, and because the differences are less than 8.51%, we can conclude that the rationality and validity of the proposed approach for calculating stresses on the right side of shallow tunnels are well verified by the numerical results. As shown in Fig. 13, gravity has a slight effect on the stresses, and its influence on the vertical normal stresses is larger than that on the horizontal normal stresses (σ_x) and shear stresses (τ_{xz}). The average differences of vertical normal stress, horizontal normal stresses and shear stresses calculated by numerical methods (considering gravity and ignoring gravity) are 6.67%, 3.21% and 3.56%, respectively.

5.2.2 Displacements and stress on the horizontal ground surface

Displacements and stress of the surrounding rock at calculation point q(D,0,0) on the horizontal ground surface calculated by the proposed approach and the numerical methods under non-axisymmetric displacement boundary conditions on a vertical surface are shown in Fig. 14 and Fig. 15, respectively, where D is the horizontal coordinate of the horizontal ground surface.

As shown in Fig. 14, the variation trends of horizontal and vertical displacements calculated by the proposed approach agree well with those by the numerical method. In

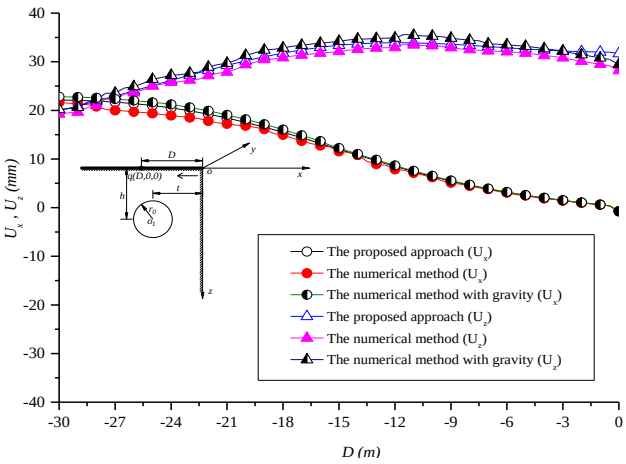

Fig. 14 Displacements of the horizontal ground surface calculated by the two methods

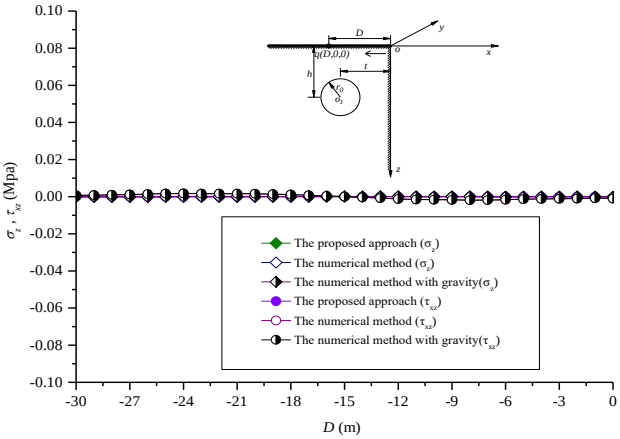

Fig. 15 Stresses on the horizontal ground surface solved by the two methods

addition, the differences of the horizontal and vertical displacements between the proposed approach and the numerical method are small. For example, the maximum differences of the horizontal and vertical displacements calculated by the two methods are 6.59% and 7.61%, respectively. Therefore, the rationality and validity of the proposed approach for calculating the displacements of the horizontal ground surface are well verified by the numerical results. As shown in Fig. 14, gravity has a slight effect on the displacements of the horizontal ground surface at calculation point q (D, 0, 0), and its influence on the vertical displacement is larger than that on the horizontal displacement. The average differences of horizontal and vertical displacements calculated by numerical simulations with and without considering gravity are 4.05% and 7.63%, respectively.

By substituting $q(D,0,0)$ into the Eqs. (9), (28), (44) and (57), the vertical normal stresses (σ_{z1}, σ_{z2}, σ_{z3}, σ_{z4}) can be obtained. Then, the values of the vertical normal stresses (σ_z) can be calculated by substituting the values of σ_{z1}, σ_{z2}, σ_{z3}, σ_{z4} into Eq. (63). In addition, by substituting $q(D,0,0)$ into the Eqs. (10), (29), (45) and (58), the shear stresses (τ_{xz1}, τ_{xz2}, τ_{xz3}, τ_{xz4}) can be obtained. Then, the values of the shear stresses (τ_z) can be calculated by substituting the values of τ_{xz1}, τ_{xz2}, τ_{xz3}, τ_{xz4} into Eq. (64). The results of the stresses on the horizontal ground surface solved by two methods are shown in Fig. 15.

As shown in Fig. 15 the vertical normal stress and shear stress on the horizontal ground surface calculated by the proposed approach and numerical methods are both zero. Thus, the rationality and validity of the proposed approach for calculating stresses on the horizontal ground surface are well verified by the numerical simulation results. In addition, gravity has a slight effect on the stresses on the horizontal ground surface, and its influence on the vertical normal stresses is larger than that on vertical ground surface at calculation point q (D,0,0). The average differences of vertical normal stresses provided by the numerical simulations between considering gravity and ignoring gravity are 6.56%, and 3.12% for the shear stresses, respectively.

6. Discussion

Generally, the horizontal ground settlement, which is defined as the ground settlement of the horizontal ground surface and caused by the shallow tunnel excavation, is an important engineering indicator to control the safety of shallow tunnels under the non-axisymmetric displacement boundary condition of a vertical surface. Therefore, the discussion will mainly focus on the effects of different tunnel buried depths, and limb distances on the unrevised and revised horizontal ground settlement shown in Fig. 16 and Fig. 17.

6.1 Effects of the tunnel buried depths on the horizontal ground settlement

To investigate the effects of different tunnel buried depths on the unrevised and revised horizontal ground settlements of the proposed approach, the horizontal ground settlements with different tunnel buried depths (i.e., h=10 m, 13 m, 16 m and 19 m) at point $q(D,0,0)$ are shown in Fig. 16. The calculation parameters are t=15 m, r_0=4.25 m, u_0=0.058 m, E=35 MPa, and v=0.5, where $U_z(D,0,0)$ is the horizontal ground settlement at point $q(D,0,0)$.

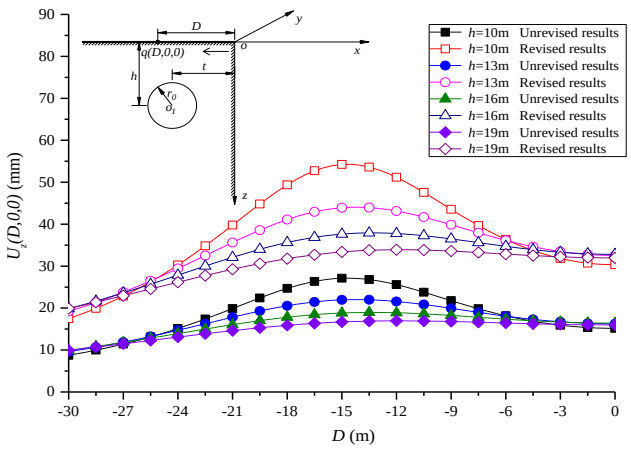

Fig. 16 Effects of tunnel buried depth on the unrevised and revised horizontal ground settlement

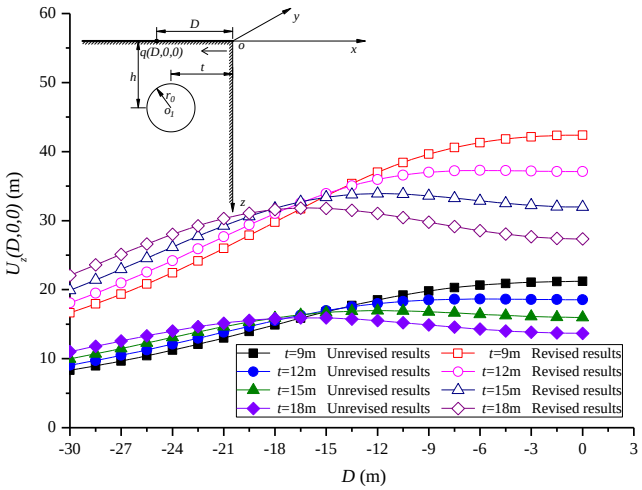

Fig. 17 Effects of limb distances on the unrevised and revised horizontal ground settlement

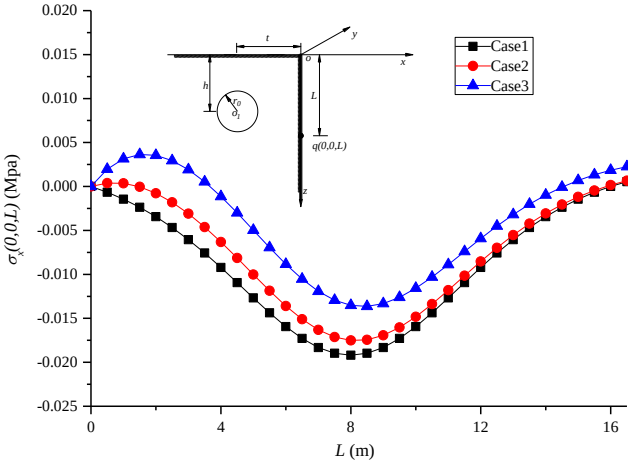

Fig. 18 Effects of limb distances on the unrevised and revised horizontal ground settlement

In Fig. 16, with increases of the tunnel buried depth, the unrevised and revised results of the horizontal ground settlement decreases gradually. For example, when the tunnel buried depth increases from 10 m to 19 m, the revised result of the maximum horizontal ground settlement falls from 54.2 mm to 33.4 mm. Therefore, the reduction percentage of the revised results of horizontal ground settlement is 38.4% when h increases from 10 m to 19 m. In addition, the differences between the unrevised and revised horizontal ground settlement remains constant with the increase of the tunnel buried depth. For example, when the tunnel buried depths are 10 m, 13 m, 16 m and 19 m, the revised results of the maximum horizontal ground settlement are larger than those of the unrevised results by 50%.

6.2 Effects of the limb distances on the horizontal ground settlement

To study the effects of different limb distances on the unrevised and revised horizontal ground settlement values of the proposed approach, the horizontal ground settlements with different limb distances (i.e., t=9 m, 12 m, 15 m and 18 m) at point $q(D,0,0)$ are shown in Fig. 17. And the calculation parameters are t=15 m, r_0=4.25 m, u_0=0.058 m, E=35 MPa, and v=0.5.

It can be seen in Fig. 17 that the unrevised and revised results of the horizontal ground settlement first decreases and then increases with increasing values of the limb distance. For example, when the limb distance increases from 9 m to 18 m, the revised horizontal ground settlements increase from 16.66 mm to 22.06 mm in the case that D is equal to -30 m, and the revised horizontal ground settlements fall from 42.38 mm to 27.35 mm in the case that D is equal to 0 m. In addition, the differences of the unrevised and revised horizontal ground settlements also remain constant with increases of the limb distance. For example, when the limb distances are 8 m, 11 m, 14 m and 17 m, the revised results of the maximum horizontal ground settlement are larger than those of the unrevised results by 50%.

6.3 Effects of the stress correction of the horizontal ground surface on the vertical surface

To investigate the stress distributions on the vertical surface after stress correction of the horizontal ground surface, three cases are taken into consideration to solve the normal stresses of vertical surface by the proposed approach. In Case 1, the horizontal normal stress of the vertical surface is obtained without considering the effect of the vertical normal and shear stresses correction on the horizontal ground surface. In Case 2, the horizontal normal stress of the vertical surface is obtained by only considering the effect of the vertical normal stress correction on the horizontal ground surface. In Case 3, the horizontal normal stress of the vertical surface is obtained by incorporating the effects of the vertical normal and shear stress correction on the horizontal ground surface. The calculation parameters are as follows: t=15 m, r_0=4.25 m, u_0=0.058 m, E=35 MPa and v=0.5. Where σ_x (0,0,L) is the horizontal normal stress of vertical surface at point $q(0,0,L)$, the calculation results are shown in Fig. 18.

The calculation results show that there are no new shear stresses, but horizontal normal stresses are generated on the vertical surface after the correction of the stress on horizontal ground surface. Fig. 18 shows that the new horizontal normal stresses for Case 3 and Case 2 are smaller than those of Case 1. The difference between Case 1 and Case 2 is 8.80%, while it is 19.2% between Case1 and Case 3. Therefore, ignoring stresses correction results in an overestimate and is more suited to deal with tunnel engineering problems when lacking engineering experience.

7. Conclusions

Based on the virtual image technique, the stress harmonic function, the stress function solution, the Boussinesq's solution and the linear superposition principle, this study presents a new approach to calculate the displacements and stresses of the surrounding rock, the ground settlements and lateral displacements of the

horizontal and vertical ground surfaces when a shallow tunnel is excavated under non-axisymmetric displacement boundary conditions. Compared with previous approaches, the following improvements have been achieved.

(1) The proposed approach extends the cavity contraction theory of the non-axisymmetric displacement boundary condition, which could reflect the 'boundary effect' of the horizontal and vertical ground surfaces.

(2) The proposed approach could provide a theoretical basis for the surrounding rock stability of the shallow tunnel excavation under non-axisymmetric displacement boundary conditions on a vertical surface.

(3) The proposed approach can be used to predict the ground settlements and lateral displacements of the horizontal and vertical ground surfaces induced by shallow tunnel excavations under non-axisymmetric displacement boundary conditions on a vertical surface.

In comparison with unrevised cases, the revised horizontal ground settlement is more conservative, which is suitable for engineering practice. The proposed approach effectively addresses bias tunnel engineering problems when construction experience is not sufficient.

8. Limitations

Although the proposed approach is presented based on some assumptions for shallow tunnels excavated under non-axisymmetric displacement boundary conditions on a vertical surface, there are still some limitations that are described as follows.

(1) The effects of the stress correction on the tunnel wall boundary are ignored.

(2) The cylindrical cavity contraction problem is considered to be a plane-strain problem and the effect of the axial displacement is neglected.

(3) The interaction influence between the horizontal ground surface and the vertical ground surface is not considered in the proposed approach.

(4) The proposed approach only takes the elasticity of the soil mass into consideration, ignoring the plastic and viscous properties of the soil mass.

(5) This paper mainly focuses on the case where the ground surface is perpendicular to the slope surface.

Acknowledgment

This work was supported by Guizhou Provincial Science and Technology Major Project, No. Qian-ke-he-zhong-da-zhuan-xiang-zi [2018]3010.

References

Alonso, E., Alejano, L.R., Varas, F., Fdez-Manin, G. and Carranza-Torres, C. (2003), "Ground response curves for rock masses exhibiting strainsoftening behavior", *Int. J. Numer. Anal. Meth. Geomech.*, **27**(13), 1153-1185. https://doi.org/10.1002/nag.315.

Boussinesq, J. (1885), *Application des Potentiels a L'Equilibre et des Mouvements des Solides Elastiques*, Gauthier-Villars, Paris, France.

Broere, W. and Van T.A.F. (2000), *Influence of Infiltration and Groundwater Flow on Tunnel Face Stability*, in *Geotechnical Aspects of Underground Construction in Soft Ground*, 339-344.

Brown, E.T., Bray, J.W., Ladanyi, B. and Hoek, E. (1983), "Ground response curves for rock tunnels", *J. Geotech. Eng.*, **109**(1), 15-39. https://doi.org/10.1061/(ASCE)0733-9410(1983)109:1(15).

Chen, G.H., Zou, J.F. and Qian, Z.H. (2019a), "An improved collapse analysis mechanism for the face stability of shield tunnel in layered soils", *Geomech. Eng.*, **17**(1), 97-107. https://doi.org/10.12989/gae.2019.17.1.097.

Chen, G.H., Zou, J., Min, Q., Guo, W.J. and Zhang, T.Z. (2019b), "Face stability analysis of a shallow square tunnel in non-homogeneous soils", *Comput. Geotech.*, **114**, 103-112. https://doi.org/10.1016/j.compgeo.2019.103112.

Daraei, A. and Zare, S. (2018), "A new strain-based criterion for evaluating tunnel stability", *Geomech. Eng.*, **16**(2), 205-215. https://doi.org/10.12989/gae.2018.16.2.205.

Farmer, I.W. and Glossop, N.H. (1979), "Settlement associated with removal of compressed air pressure during tunnelling in alluvial clay", *Geotechnique*, **29**(1), 67-72. https://doi.org/10.1680/geot.1979.29.1.67.

Fahimifar, A.; Ghadami, H. and Ahmadvand, M. (2015), "The ground response curve of underwater tunnels, excavated in a strain-softening rock mass", *Geomech. Eng.*, **8**(3), 323-359. http://dx.doi.org/10.12989/gae.2015.8.3.323.

Han, K.H., Zhang, C.P. and Zhang, D.L. (2016), "Upper-bound solutions for the face stability of a shield tunnel in multilayered cohesive–frictional soils", *Comput. Geotech.*, **79**, 1-9. https://doi.org/10.1016/j.compgeo.2016.05.018.

Huang M.S., Li, S., Zhou, W.X. and Yu, J.Y. (2018), "Continuous field based upper bound analysis for three-dimensional tunnel face stability in undrained clay", *Comput. Geotech.*, **94**, 207-213. https://doi.org/10.1016/j.compgeo.2017.09.014.

Kassir, M.K. and Sih, G.C. (1975), *Three-Dimensional Crack Problems*, Noordhoff International Publishing, Dordrecht, The Netherlands.

Lee, Y.K. and Pietruszczak, S. (2008), "A new numerical procedure for elasto-plastic analysis of a circular opening excavated in a strain-softening rock mass", *Tunn. Undergr. Sp. Technol.*, **23**(5), 588-599. https://doi.org/10.1016/j.tust.2007.11.002.

Li, C., Zou, J.F. and A, S.G. (2019a), "Closed-Form solution for undrained cavity expansion in anisotropic soil mass based on spatially mobilized plane failure criterion", *Int. J. Geomech.*, **19**(7), 04019075. https://doi.org/10.1061/(ASCE)GM.1943-5622.0001458.

Li, C., Zou, J.F. and Zhou, H. (2019b), "Cavity expansion in k0 consolidated clay", *Eur. J. Environ. Civ. Eng.*, 2019, 1-19. DOI: 10.1080/19648189.2019.1605937.

Loganathan, N. and Poulos, H.G. (1998), "Analytical prediction for tunneling-induced ground movements in clays", *J. Geotech. Geoenviron. Eng.*, **124**(9), 846-856. https://doi.org/10.1061/(ASCE)1090-0241(1998)124:9(846).

Li, J.P., Zhang, Y.G., Chen, H.B. and Liang, F.Y. (2013), "Analytical solutions of spherical cavity expansion near a slope due to pile installation", *J. Appl. Math.*, 1-11. http://dx.doi.org/10.1155/2013/306849.

Li, T.Z. and Yang, X.L. (2019), "Three-dimensional face stability of shallow-buried tunnels with tensile strength cut-off", *Comput. Geotech.*, **110**, 82-93. https://doi.org/10.1016/j.compgeo.2019.02.014.

Mollon, G., Dias, D. and Soubra, A.H. (2011), "Rotational failure mechanisms for the face stability analysis of tunnels driven by a pressurized shield", *Int. J. Numer. Anal. Meth. Geomech.*, **35**(12), 1363-1388. https://doi.org/10.1002/nag.962.

Mollon, G., Dias, D. and Soubra, A.H. (2013), "Continuous

velocity fields for collapse and blowout of a pressurized tunnel face in purely cohesive soil", *Int. J. Numer. Anal. Meth. Geomech.*, **37**(13), 2061-2083. https://doi.org/10.1002/nag.2121.

Oreste, P.P. and Dias, D. (2012), "Stabilisation of the excavation face in shallow tunnels using fibreglass dowels", *Rock Mech. Rock Eng.*, **45**(4), 499-517. https://doi.org/10.1007/s00603-012-0234-1.

Peck, R.B. (1969), "Deep excavations and tunneling in soft ground", *Proceedings of the 7th International Conference on Soil Mechanics and Foundation Engineering*, Mexico City, Mexico.

Park, K.H. (2004), "Elastic solution for tunneling-induced ground movements in clays", *Int. J. Geomech.*, **4**(4), 310-318. https://doi.org/10.1061/(ASCE)1532-3641(2004)4:4(310).

Pan, Q.J. and Dias, D. (2017), "Upper-bound analysis on the face stability of a non-circular tunnel", *Tunn. Undergr. Sp. Technol.*, **62**, 96-102. https://doi.org/10.1016/j.tust.2016.11.010.

Pan, Q.J. and Dias, D. (2018), "Three dimensional face stability of a rock tunnel subjected to seepage forces" *Tunn. Undergr. Sp. Technol.*, **71**, 555-566. https://doi.org/10.1016/j.tust.2017.11.003.

Timoshenko, S.P. and Goodier, J.N. (1970), *Theory of Elasticity*, McGraw Hill, New York, U.S.A.

Verruijt, A. (1997), "A complex variable solution for a deforming circular tunnel in an elastic half plane", *Int. J. Numer. Anal. Meth. Geomech.*, **21**(2), 77-89. https://doi.org/10.1002/(SICI)1096-9853(199702)21:2%3C77::AID-NAG857%3E3.0.CO;2-M.

Verruijt, A. (1998), "Deformations of an elastic half plane with circular cavity", *Int. J. Solid. Struct.*, **35**(21), 2795-2804. https://doi.org/10.1016/S0020-7683(97)00194-7.

Wood, A.M.M. (1975), "Circular tunnel in elastic ground", *Geotechnique*, **25**(1), 115-127. https://doi.org/10.1680/geot.1975.25.1.115.

Wang, S., Yin, K., Tang, Y.H. and Ge, X. (2010), "A new approach for analyzing circular tunnel in strain-softening rock masses", *Int. J. Rock Mech. Min. Sci.*, **47**(1), 170-178. http://dx.doi.org/10.1016%2Fj.ijrmms.2009.02.011.

Wang, L., Zou, J.F. and Sheng, Y.M. (2019), "An improved stress and strain increment approaches for circular tunnel in strain-softening surrounding rock considering seepage force", *Adv. Mater. Sci. Eng.* https://doi.org/10.1155/2019/2075240.

Xiao, Y., Sun, Y., Yin, F., Liu, H. and Xiang, J. (2017a), "Stress-strain-strength response and ductility of gravels improved by polyurethane foam adhesive", *J. Geotech. Geoenviron. Eng.*, **144**(2), 04017108. https://doi.org/10.1061/(ASCE)GT.1943-5606.0001812.

Xiao, Y., Sun, Y., Yin, F., Liu, H. and Xiang, J. (2017b), "Constitutive modeling for transparent granular soils", *Int. J. Geomech.*, **17**(7), 04016150. https://doi.org/10.1061/(ASCE)GM.1943-5622.0000857.

Yu, H.S. and Houlsby, G.T. (1995), "Large strain analytical solution for cavity contraction in dilatant soils", *Int. J. Numer. Anal. Meth. Geomech.*, **19**(11), 793-811. https://doi.org/10.1002/nag.1610191104.

Yu, H.S. and Rowe, R.K. (1999), "Plasticity solutions for soil behavior around contracting cavities and tunnels", *Int. J. Numer. Anal. Meth. Geomech.*, **23**(12), 1245-1279. https://doi.org/10.1002/(SICI)1096-9853(199910)23:12%3C1245::AID-NAG30%3E3.0.CO;2-W.

Yu, H.S. and Carter, J.P. (2002), "Rigorous similarity solutions for cavity expansion in cohesive-frictional soils", *Int. J. Geomech.*, **2**(2), 233-258. https://doi.org/10.1061/(ASCE)1532-3641(2002)2:2(233).

Zhang, C., Han, K. and Zhang, D. (2015), "Face stability analysis of shallow circular tunnels in cohesive-frictional soils", *Tunn. Undergr. Sp. Technol.*, **50**, 345-357. https://doi.org/10.1016/j.tust.2015.08.007.

Zhang, F., Gao, Y.F., Wu, Y.X. and Zhang, N. (2018), "Upper-bound solutions for face stability of circular tunnels in undrained clays", *Géotechnique*, **68**(1), 1-13. https://doi.org/10.1680/jgeot.16.T.028.

Zou, J.F. and Zuo, S.Q. (2017), "Similarity solution for the synchronous grouting of shield tunnels under the non-axisymmetric displacement boundary on vertical surface", *Adv. Appl. Math. Mech.*, **9**(1), 205-232. https://doi.org/10.4208/aamm.2016.m1479.

Zou, J.F., Liu, S.X., Li, J.B. and Qian, Z H. (2019a), "Face stability analysis for a shield-driven tunnel with non-linear yield criterion", *Proc. Inst. Civ. Eng. Geotech. Eng.*, **172**(3), 243-254. https://doi.org/10.1680/jgeen.17.00222.

Zou, J.F., Qian, Z.H., Xiang, X.H. and Chen, G.H. (2019b), "Face stability of a tunnel excavated in saturated nonhomogeneous soils", *Tunn. Undergr. Sp. Technol.*, **83**(1), 1-17. https://doi.org/10.1016/j.tust.2018.09.007.

Zou J.F., Wang, F. and Wei, A. (2019c), "A semi-analytical solution for shallow tunnels with radius-iterative-approach in semi-infinite space", *Appl. Math. Modell.*, **73**(9), 285-302. https://doi.org/10.1016/j.apm.2019.04.007.

Zou, J.F., Yang, T., Wang, L., Guo, W.J. and Huang, F.L. (2019d), "A numerical stepwise approach for cavity expansion problem in strain-softening rock or soil mass", *Geomech. Eng.*, **18**(3), 225-234. https://doi.org/10.12989/gae.2019.18.3.225.

CC